Mechanism of Dioxygen Activation in 2-Oxoglutarate-Dependent Enzymes: A Hybrid DFT Study

Tomasz Borowski,* Arianna Bassan, and Per E. M. Siegbahn[a]

Abstract: The reaction mechanism for dioxygen activation in 2-oxoglutarate-dependent enzymes has been studied by means of hybrid density functional theory. The results reported here support a mechanism in which all chemical transformations take place on a quintet potential-energy surface. More specifically, the activated dioxygen species attacks the carbonyl group of the co-substrate producing the Fe^{II}–persuccinate–CO_2 complex, which readily releases the carbon dioxide molecule. The step in which the Fe^{II}–peracid–CO_2 complex is formed is found to be rate-limiting and irreversible. Subsequent heterolysis of the O–O bond in the Fe^{II}–persuccinate complex proceeds in two one-electron steps and produces the high-valent iron–oxo species Fe^{IV}=O, which is most likely to be responsible for oxidative reactions catalyzed by 2-oxoglutarate-dependent enzymes. The concerted pathway for simultaneous O–O and C–C bond cleavage on the septet potential-energy surface is found to be less favorable. The relative stability of different forms of the active iron–oxo species is assessed, and the quintet five-coordinate complex is found to be most stable.

Keywords: density functional calculations · enzyme catalysis · non-heme iron enzymes · O–O activation · oxoglutarate

Introduction

Non-heme iron enzymes dependent on 2-oxoglutarate (α-ketoglutarate, abbreviated here as α-KG) constitute a large class of oxygenases that play key roles in a broad range of primary and secondary metabolic pathways. For example, prolyl hydroxylases take part in post-translational processing of collagen in animals and in the hypoxia induced factor (HIF)-mediated pathway for dioxygen sensing;[1,2] thymine 7-hydroxylase is a pivotal enzyme in pyrimidine metabolism; clavaminic acid synthase (CS) participates in clavulanic acid biosynthesis in *Streptomyces clavuligerus* bacteria; finally the newly discovered AlkB repair enzymes catalyze demethylation of alkylated DNA and RNA.[3–5] All α-KG-dependent non-heme iron enzymes require ferrous ion, α-KG, and O_2 for catalytic activity. The majority of them catalyze hydroxylation of an unactivated C–H bond coupled with an oxidative decarboxylation of the co-substrate α-KG. A number of excellent reviews on these enzymes are available in the literature, and interested readers are referred to them for further information regarding the biological functions of α-KG-dependent non-heme iron enzymes.[6–12]

Several crystal structures of α-KG-dependent enzymes have been reported (clavaminic acid synthase,[13] proline-3-hydroxylase (P-3-H),[14] anthocyanidin synthase (ANS),[15] deacetoxycephalosporin C synthase (DAOCS),[16,17] and the related 4-hydroxyphenylpyruvate dioxygenase (HPPD)[18]) all of them reveal a common 2-His-1-carboxylate facial-triad iron-binding motif characteristic of a broad group of non-heme iron enzymes.[19] In the native ferrous-ion-bound form, the remaining three coordination positions are occupied by water molecules, as exemplified by the crystal structure of the DAOCS–Fe^{II} complex[16] (PDB access code: 1RXF); this arrangement is supported by spectroscopic studies on CS.[20,21] α-KG binds to iron in a bidentate fashion, which means that two of the three water ligands initially bound to iron are displaced by the co-substrate. Crystal structures of CS–Fe^{II}–α-KG complexes[13] (with *N*-α-L-acetyl arginine, 1DRY; with proclavaminic acid, 1DRT) together with spectroscopic results[20,21] indicate that the remaining water molecule is displaced from the CS–Fe^{II}–α–KG complex upon primary substrate binding. These observations have led Solomon and co-workers to propose a general mechanism depicted in Scheme 1,[12,22] which is composed of three steps A, B, and C: step A, during which the α-KG co-substrate enters the first coordination sphere of iron, is followed by substrate binding in the vicinity of the non-heme complex (step B). Notably, the substrate perturbs the ferrous site and

[a] Dr. T. Borowski, A. Bassan, Prof. P. E. M. Siegbahn
Department of Physics, Stockholm Center for Physics Astronomy and Biotechnology, Stockholm University
106 91 Stockholm (Sweden)
Fax: (+46) 8-55378600
E-mail: borowski@physto.se

 DOI: 10.1002/chem.200305306

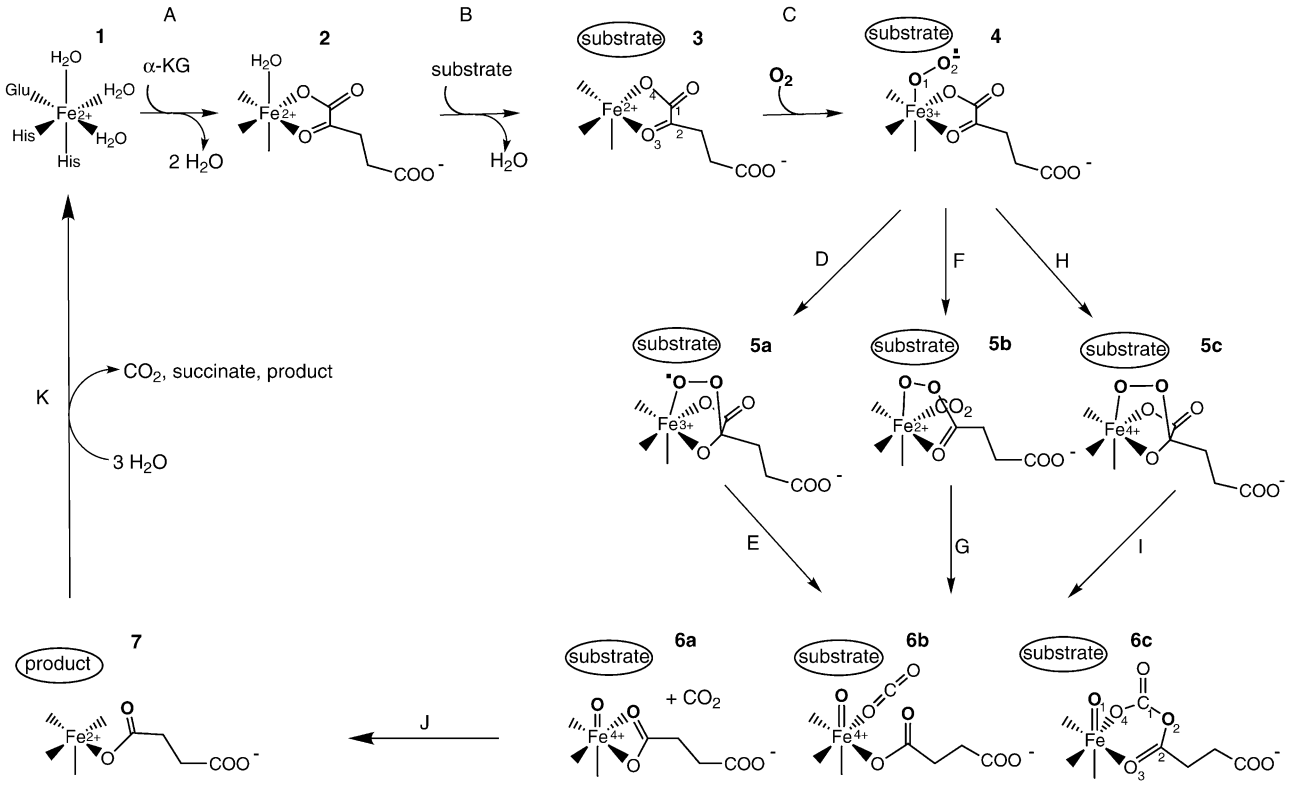

Scheme 1. Mechanisms proposed for the catalytic reaction mechanism of α-KG-dependent enzymes.

causes the displacement of the water ligand, leading to a five-coordinate iron complex. The vacancy on iron, which is necessary for O_2 activation (step C), is formed only if the substrate and co-substrate are already bound at the active site. It follows that the nonproductive so-called "uncoupled" reaction, in which oxidative decarboxylation of α-KG is not tied with oxidation of primary substrate, is greatly reduced.

As the hydroxylation reaction of an unactivated C–H bond and a broad repertoire of other reactions catalyzed by α-KG-dependent enzymes (i.e., epoxidation of olefins, oxidation of sulfides to sulfones and sulfoxides and oxidation of substituted methylamines)[23] mirror the chemical behavior of cytochrome P-450, it is now widely accepted that a ferryl–oxo species (Fe^{IV}=O), similar to compounds I and II characterized for heme proteins,[24,25] is formed upon the dioxygen activation step(s) of the catalytic cycle (see Scheme 1). Indeed, a high-valent iron intermediate produced in the reaction of taurine/α-KG dioxygenase has been recently identified by means of absorption, Mössbauer and EPR spectroscopy,[26] supporting a mechanism in which the ferryl species plays a key role in catalysis. Although the actual structure of this intermediate still needs to be determined, the spectroscopic results indicate that this is a high-spin ($S=2$) complex with formal oxidation state of iron equal to four.

In spite of the scarce experimental evidence about the oxygen activation process, a few mechanisms have been proposed in the literature and they are presented in Scheme 1. In the concerted mechanism (steps D and E), the carbon–carbon and oxygen–oxygen bonds in a superoxo-bridged intermediate (**5a** in Scheme 1) are cleaved simultaneously producing the ferryl–oxo intermediate (**6** in Scheme 1),[12] while in the step-wise mechanism (steps F and G) these two bonds are cleaved in two consecutive steps.[9] First the C–C bond is broken generating a Fe^{II}–peracid complex and CO_2 (step F); in the second step (step G) the O–O bond heterolysis leads to the active ferryl–oxo intermediate. With respect to this pathway, there is some experimental evidence suggesting that persuccinic acid does not bind to the α-KG-dependent enzymes.[27,28] However, this observation does not necessarily rule out the Fe^{II}–persuccinate complex as an enzymatic intermediate.[9] One possible reason could be a high pKa of a peracid making the binding to the enzyme thermodynamically unfavorable, while the Fe^{II}–persuccinate complex may be efficiently produced and consumed during the catalytic cycle. The third plausible route for dioxygen activation involves an Fe^{IV}–peroxo intermediate (step H) which decomposes into the active species (step I).[13,29] All these mechanisms are in accord with the results of isotope-labeling experiments, which have shown that one oxygen atom originating from dioxygen is incorporated into the decarboxylation product (succinate), while the second oxygen derived from O_2 is found in the hydroxylation product. Once the C–C and O–O bonds are cleaved, carbon dioxide can either dissociate from iron (**6a** in Scheme 1) or may stay in its first coordination sphere either in the "native" form (**6b**)[17] or as an anhydride with succinate (**6c**).[13,29] Oxidation of the primary substrate (step J) followed by product release (step K) completes the catalytic cycle.

Clavaminic acid synthase (CS) is one of the best characterized and most fascinating proteins from the group of α-KG-dependent enzymes. It catalyzes three separate oxida-

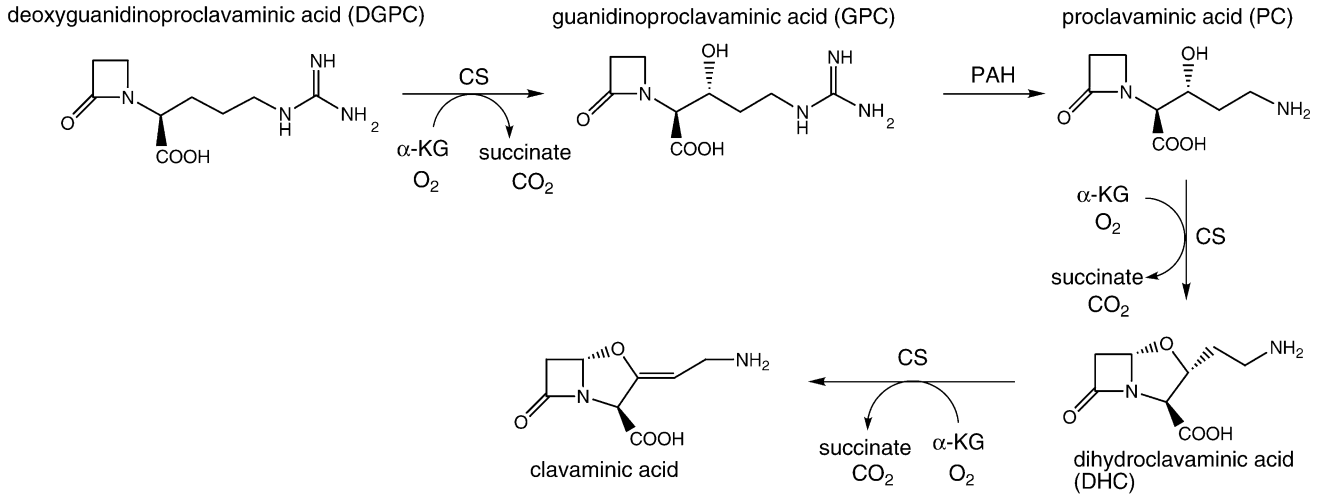

Scheme 2. The role of CS in clavaminic acid biosynthesis.

tive reactions in the biosynthesis of clavulanic acid—a potent inhibitor of serine β-lactamases that is commonly used with β-lactam antibiotics in antibacterial treatment. As shown in Scheme 2, the first hydroxylation reaction is separated from the subsequent cyclization and desaturation by hydrolysis of the guanidino group, which is catalyzed by proclavaminate amidinohydrolase (PAH).

The crystal structure of CS has been solved for several different forms: the apo form (PDB access code: 1DS0), the CS-Fe^{II}–α–KG complex (1DS1), the CS–Fe^{II}–α-KG–PC complex (PC = proclavaminic acid; 1DRT), the CS–Fe^{II}–α-KG–*N*-α-NAA complex (NAA = *N*-α-L-acetyl arginine; 1DRY), and the CS–Fe^{II}–α-KG–NO–DGPC complex (DGPC = deoxyguanidinoproclavaminic acid; 1GVG). The active site region of the CS–Fe^{II}–α-KG–NAA complex is depicted in Figure 1. Note that the ferrous ion is coordinated by six atoms in a roughly octahedral arrangement. His144 and His279 together with Glu146 supply three atoms for one face of the octahedron, while α-KG and water487 fill the three remaining positions. Two second-shell ligands, Tyr299 and Arg279, form hydrogen bonds with the carboxylic groups of Glu146 and α-KG. The water ligand bound *trans* to His279 is supposedly replaced by O_2 after binding of the primary substrate. Therefore, after dioxygen activation, the oxo group would occupy this position, which is ideal for performing further catalytic steps. However, the structure of the CS–Fe^{II}–α-KG–NO–DGPC complex (DGPC = deoxyguanidinoproclavaminic acid, substrate for the hydroxylation reaction shown in Scheme 2) reveals that nitric oxide binds to iron at the position *trans* to His144, while the 1-carboxylic group of α-KG occupies a position opposite to His279.[30] Thus, at the present time, the precise location of O_2 binding in the iron complex of CS remains obscure, as either NO may be an imperfect analogue of dioxygen, or some rearrangement may take place after the oxygen activation.

Model systems mimicking the chemistry of α-KG-dependent enzymes have been synthesized. Comparison of coordinatively saturated and unsaturated model systems has showed that the latter react with dioxygen much faster,

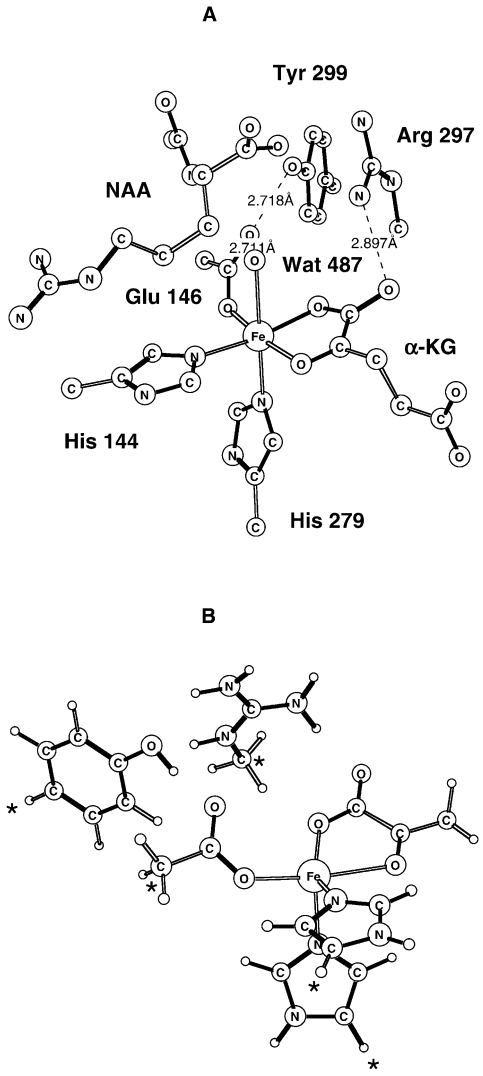

Figure 1. The X-ray structure (1DRY) of the active site of CS (A) and the model used in the calculations (B). Atoms marked with an asterisk have had fixed positions in the optimizations.

demonstrating the importance of a vacant position at the ferrous ion.[31,32] In line with this experimental evidence, it has been proposed that dioxygen binds at this vacant position to iron and forms a ferrous-superoxo species (Fe^{3+}–$O_2^{\bullet-}$), which then performs a nucleophilic attack on the carbonyl carbon of the α-keto acid. The nucleophilic character of this reaction is supported by kinetic measurements performed for various derivatives with different substituents in the α-keto acid moiety.[31,33] The more electron withdrawing the group bound in this fragment is, the faster is the reaction between the complex and dioxygen. In line with this argument there is experimental evidence showing that superoxide is a potent nucleophile[34] capable of cleaving α-keto carboxylic acids.[35] As the biomimetic complexes catalyze olefin epoxidation[32] and aryl hydroxylation,[36,37] the ferryl–oxo intermediate has been proposed to be responsible for the oxidative chemistry in these non-heme iron systems. Interestingly, such a ferryl–oxo non-heme iron species has recently been synthesized and characterized by Que, Jr. and co-workers.[38]

In this work, hybrid density functional methods have been used to elucidate the mechanism of oxygen activation utilized by α-KG-dependent enzymes. The clavaminic acid synthase (CS) has been chosen as a system of interest, because, firstly, several high resolution crystal structures are available for various forms of this enzyme (vide supra), and secondly, because the spectroscopic measurements done for CS have clearly demonstrated that the active site iron becomes five-coordinate upon binding of the primary substrate. The steps following five-coordinate Fe^{II} site formation and leading to the active ferryl–oxo species (steps leading from species **3** to **6** in Scheme 1) have been studied and the results are reported in the following subsections.

Computational Methods

In the present work, a model based on the crystal structure of the CS–Fe^{II}–α-KG complex (PDB access code: 1DS1) was employed (see Figure 1B). This particular crystal structure was chosen, since it has been solved to the highest resolution (1.08 Å) among all structures of α-KG-dependent enzymes.[13] In the initial model used in the calculations, the water molecule (Wat 487 in Figure 1A), which coordinates the ferrous ion in the crystal structure, was removed. This structural change was introduced in order to model a five-coordinate non-heme iron active site, which is capable to react with dioxygen. In this way the influence of the substrate on the geometry of the iron site was indirectly taken into account. Notably, the crystal structure of the enzyme–Fe^{II}–α-KG–substrate analogue complex indicates that only the chemically inert C–H bond of the substrate points in the direction of the putative dioxygen binding site. Therefore, the substrate does not seem to play any active role in dioxygen activation (steps D–I, Scheme 1) and it was not included in the calculations. The model was composed of a ferrous ion together with groups modeling the most relevant first and second coordination shell ligands (see Figure 1). Specifically, the co-substrate was modeled by pyruvate, histidines by imidazole rings, glutamate by acetate, while the second shell ligands tyrosine and arginine were represented by phenol and methyloguanidino groups, respectively. In order to prevent unrealistic geometry changes during the geometry optimizations some constraints were imposed on the residues. More specifically, the atoms marked with an asterisk in Figure 1B were fixed to their positions in the X-ray structure. This procedure should guarantee that the optimized structures have reasonable geometries. Previous studies have indicated that this approach gives reliable results as the constraints introduce only a small energy correction (less than 2 kcal mol^{-1}) in comparison to the fully optimized models.[39] Since the applied constraints made an harmonic analysis not rigorously valid, a second, much smaller model was used to assess the thermal effects of the reactions. In the small model, histidines were replaced by ammonia molecules, and glutamate by formate, while the second shell ligands were omitted.

All calculations were performed by employing hybrid density functional theory (DFT) with the B3LYP[40,41] exchange-correlation functional. Two programs, Gaussian[42] and Jaguar,[43] were used to investigate the chemical transformations occurring in the active site of α-KG-dependent enzymes during O_2 activation. Geometry optimizations and molecular Hessian calculations were performed with a valence double-zeta basis set coupled with an effective core potential, describing the innermost electrons on iron. This particular basis set is labeled lacvp in Jaguar. For the optimized structures the electronic energy was computed with a bigger basis set of triple-zeta quality with polarization functions on all atoms (labeled lacv3p** in Jaguar). The solvent corrections were calculated with the self-consistent reaction field method implemented in Jaguar.[44,45] A dielectric constant of 4 with a probe radius of 2.5 Å were assumed. All transition-state optimizations and Hessian calculations were performed with Gaussian 98 and the thermal corrections were calculated for the temperature of 298.15 K.

Finally, a comment should be made about the reference system chosen for the energetic considerations. Previous theoretical studies on hemerythrin have implicated that an accurate calculation of the dioxygen binding energy is a very demanding task.[46] It has been found that a QM/MM approach is necessary to estimate the O_2 binding energy with satisfactory agreement with experimental data. A detailed theoretical analysis has shown that the free energy of the binding of O_2 to hemerythrin (non-heme iron enzyme) is significantly affected by van der Waals and electrostatic contributions from the protein environment. These two types of interactions, which cannot be described by the models used in this work, contribute almost -10 kcal mol^{-1} to the free energy of O_2 binding, and almost cancel the significant entropy effects due to the trapping of molecular oxygen by the metal complex. In the present study, the binding of O_2 to the iron center of α-KG-dependent enzymes was computed to be endergonic by 9.3 kcal mol^{-1} (without solvent effects), and it was assumed that, in analogy to the hemerythrin case, this energy is cancelled by the van der Waals and electrostatic effects in the protein, leading to a thermoneutral or only slightly endergonic O_2 binding. Accordingly, the free energy of the triplet Fe–O_2 complex serves as a reference point, and all energies reported in this work, if not stated otherwise, are relative free energies calculated with respect to this structure.

Results and Discussion

The present study focuses on dioxygen activation by the non-heme iron enzymes from the group of α-KG-dependent dioxygenases. The dioxygen activation process, which leads from structure **3** to **6** in Scheme 1, is formally a four-electron reduction of O_2 by the Fe^{II}–α-KG complex. Two electrons necessary for this reaction are supplied by iron, which changes its oxidation state from $+2$ to $+4$, while the remaining two electrons originate from the co-substrate undergoing oxidative decarboxylation. Because several different scenarios seem plausible for this process, the theoretical investigation was undertaken with the hope of gaining further insight into this intricate redox process. Thus, in the following subsections the results obtained for the elementary steps comprising the O_2 activation process are described with special emphasis on the electronic structure changes taking place along the reaction coordinate. Specifically, the properties of the five-coordinate ferrous active complex and binding of dioxygen to iron are discussed in the first two subsec-

tions. Then, the co-substrate decarboxylation is addressed and is followed by a subsection devoted to the O–O bond heterolysis. Finally, the stability of different forms of the high-valent iron-oxo species is discussed.

Five-coordinate iron site: Since spectroscopic studies on CS[20,21] and model systems[32,36] have indicated that the iron complex must be five-coordinate to bind dioxygen efficiently, the five-coordinate complex, corresponding to species **3** in Scheme 1 and depicted in Figure 1B, has been chosen as a starting point for the calculations. The optimized structure

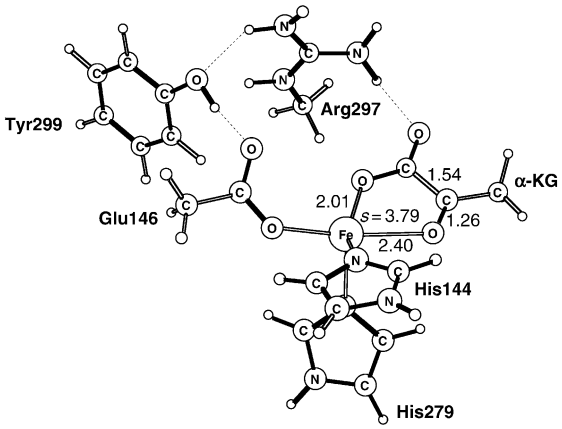

Figure 2. Optimized structure for the quintet ground state of the penta-coordinate ferrous complex with α-KG in the first coordination shell.

of this species is shown in Figure 2, in which the spin population on iron and the most relevant interatomic distances are also presented. In Figure 2 it is apparent that the co-substrate binds to iron in a bidentate manner. However, the distance between iron and the α-keto oxygen atom increases upon water ligand release (the Fe–O3 distance is 2.21 Å in the crystal structure of the six-coordinate species and 2.40 Å in the optimized five-coordinate species; for atoms numbering see Scheme 1). This iron–carbonyl-oxygen bond elongation is in agreement with the crystallographic data obtained for CS–Fe^{II}–α-KG–substrate complexes, in which the water ligand binding is either perturbed (1DRY) or the water is completely displaced from the coordination sphere of iron (1DRT). In these two crystal structures the Fe–O3 distance amounts to 2.25 Å and 2.54 Å, respectively, and the latter value is close to that from the optimized model complex (2.40 Å). It seems probable, that the Fe–O3 bond elongation is caused by a *trans*-effect due to a stronger interaction between Glu146 and Fe^{II} in a five-coordinate species. All the other metal–ligand distances change only slightly upon water release, and the geometry of the complex is best described as square pyramidal with His279 as an axial ligand. The ferrous ion is in a quintet high-spin state, which is typical for non-heme iron enzymes usually providing ligands producing a weak ligand field on Fe^{II}.[12]

Dioxygen binding to the non-heme iron site: All mechanisms proposed in the literature for α-KG-dependent enzymes suggest that dioxygen binds to iron and becomes activated for further catalytic steps (species **4** in Scheme 1). Oxygen activation might, for example, involve an electron transfer from iron(II) leading to a ferric-superoxide species. Due to the open-shell character of the iron site and dioxygen, several spin states are possible for the Fe–O_2 complex, and this diversity has to be taken into account when modeling the catalytic reaction of α-KG-dependent enzymes. Specifically, the septet, quintet, and triplet spin states for the iron–dioxygen complex have been explored. The relative energies and most interesting spin populations and bond lengths obtained for these complexes are gathered in Table 1, and the structure of the quintet complex is presented in Figure 3. Inspection of Table 1 reveals that for the Fe–

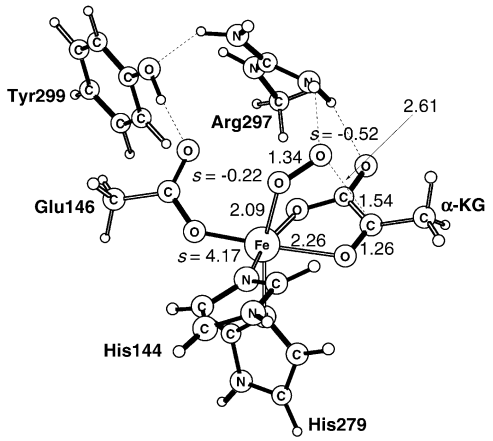

Figure 3. Optimized structure for the iron–dioxygen complex in the quintet spin state.

O_2 complex three different spin states lie close in energy. The triplet state has the lowest energy and also the longest iron–oxygen bond length. The spin distribution for that complex reveals that the iron is in a ferrous high-spin state, while the loosely bound dioxygen retains its triplet character. Excitation to the septet and quintet spin states promotes some charge shift from iron to dioxygen. From the spin populations reported in Table 1 it can be inferred that for these two spin states, iron is in a ferric oxidation state and the dioxygen fragment gains superoxide character. It is also interesting to note, that the amount of charge transfer from iron to dioxygen, as shown by the spin distribution, increases in the order: triplet, septet, quintet and follows the increase of the O–O bond length and the decrease of the Fe–O bond length. Moreover, the largest negative charge accumulated on the iron-bound dioxygen in the quintet complex is also

Table 1. Relative energies and chosen metric parameters for optimized iron–dioxygen complexes.

Multiplicity	ΔG [kcal mol^{-1}]	ΔH [kcal mol^{-1}]	$-T\Delta S$ [kcal mol^{-1}]	Fe–O1 [Å]	O1–O2 [Å]	Spin on Fe	Spin on O1	Spin on O2
septet	2.2	0.9	1.3	2.28	1.31	4.06	0.76	0.76
quintet	5.8	1.8	4.0	2.09	1.34	4.17	−0.22	−0.52
triplet	0.0	0.0	0.0	2.30	1.26	3.71	−0.92	−0.97

reflected by the sum of the Mulliken charges on the two oxygen atoms, which amounts to: −0.28, −0.44, and 0.00, for the septet, quintet, and triplet states, respectively.

Attack of the activated oxygen species on the α-keto group of the co-substrate: As has already been indicated, in the quintet state of the Fe–O_2 complex the dioxygen fragment attains the largest negative partial charge, and the electronic structure of this complex is best described by the Fe^{3+}–$O_2^{\bullet-}$ formula. It is interesting to note that there is experimental evidence[34,35] indicating that the superoxide ion is a potent nucleophile capable of oxidative decarboxylation of α-keto acids. In addition, studies on model systems[31,33] support a nucleophilic character of the rate-limiting step in the oxidative decarboxylation of the α-keto acid. Taking this into account, the quintet spin state of Fe–O_2 seems to be the most appropriate starting point for the next elementary step in the catalytic reaction. Therefore, the quintet potential-energy surface (PES) has been explored first, and the following scenario for dioxygen activation has emerged from the computational results (see Figure 11, vide infra, for the free-energy profile along the reaction coordinate). Reduction of dioxygen by the co-substrate starts with the attack of the ferric–$O_2^{\bullet-}$ species on the carbonyl group of the α-keto acid. In this step, a new C–O bond is formed, while simultaneously the C–C bond of α-KG is cleaved. Notably, all attempts to optimize the structure of an intermediate with either a superoxo or a peroxo bridge between iron and the co-substrate (**5a** and **5c** in Scheme 1) failed for the quintet PES. It follows that the elementary step F in Scheme 1, which leads to the Fe^{II}-peracid intermediate (**5b**), has been found to be the most plausible route for the productive decay of the iron–oxygen complex.

The structure of the optimized transition state leading to the iron(II)–peracid intermediate is shown in Figure 4, in which the most relevant spin populations and bond lengths are reported. The spin on iron (4.20) is only slightly increased, while the spin polarization on the dioxygen fragment is reversed with respect to the preceding iron–dioxygen complex in Figure 3. Some transient spin also builds up on the carbonyl oxygen of the co-substrate. As regards the geometry of this transition state, comparing the bond lengths in Figures 3 and 4, we notice that the iron–oxygen and carbon–carbon bonds are significantly elongated with respect to the Fe^{3+}–$O_2^{\bullet-}$ structure. Notably, the carbon–oxygen bond, which is formed in this step, has already a length characteristic of a single C–O bond. The critical bond lengths and spin populations for the transition state indicate that at this point on the potential-energy surface the dioxygen fragment still has a superoxide character, while iron is in the ferric oxidation state. Therefore, the chemical character of the process leading from the Fe–O_2 complex to this transition state is best described as a nucleophilic attack of the superoxide species on the α-keto group of the co-substrate. This observation is in agreement with experimental data obtained for biomimetic complexes.[32,33] Once the transition state is passed, the electronic structure rearranges as the oxidative decarboxylation of α-KG supplies two electrons needed for the reduction of Fe^{3+}–$O_2^{\bullet-}$ to the Fe^{2+}–peroxo species. The calculated free energy for this transition state is 16.1 kcal mol^{-1}, which partitions into an enthalpy of 9.7 kcal mol^{-1} and a $-T\Delta S$ term of 6.4 kcal mol^{-1}. This theoretical estimate of the activation free energy compares favorably with the experimental kinetic data obtained for taurine/α-KG dioxygenase.[47] In that case the rate constant for the reaction between the enzyme–Fe^{II}–α-KG–taurine complex and dioxygen is $42 \pm 9\ s^{-1}$, which corresponds to a barrier of 15.2 kcal mol^{-1}. A slightly larger activation free energy (18.8 kcal mol^{-1}) has been found for a model system,[33] in which the major contribution to the activation energy originates from the entropy term ($\Delta H = 6.0$ kcal mol^{-1}, $-T\Delta S = 12.8$ kcal mol^{-1}). The transition state shown in Figure 4 decays to the Fe^{II}–peracid–CO_2 complex (see Figure 5), which lies 41.1 kcal mol^{-1} ($\Delta H = -40.7$ kcal mol^{-1}, $-T\Delta S = -0.4$ kcal mol^{-1}) below the reactant. The high exergonicity of this reaction shows that this catalytic step is irreversible at physiological temperatures.

The spin distribution and bond lengths for the iron(II)-peracid intermediate (Figure 5) indicate that the C–C bond cleavage leads to the reduction of the ferric–superoxo moiety to the ferrous–peroxo one. The structural arrangement of this intermediate shows a distance between the ferrous ion and carbon dioxide significantly longer than that

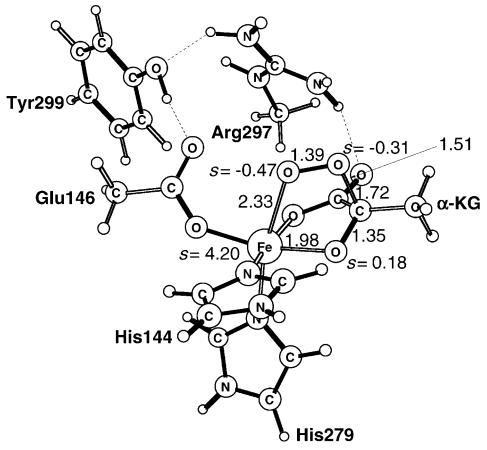

Figure 4. Optimized structure for the quintet transition state leading to the formation of the ferrous–peracid complex.

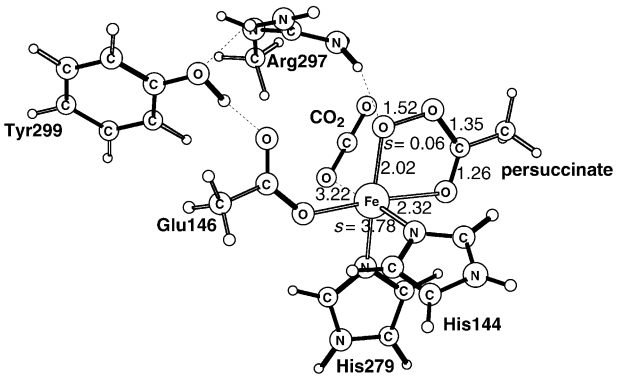

Figure 5. Optimized structure for the quintet ground state of the Fe^{II}–peracid–CO_2 complex.

corresponding to a usual coordination bond. This observation suggests a weak interaction between CO_2 and the ferrous center. In fact, when carbon dioxide is removed from this complex, the calculated free energy for CO_2 release is $-9.7\ kcal\,mol^{-1}$ ($\Delta H = -1.5\ kcal\,mol^{-1}$, $-T\Delta S = -8.2\ kcal\,mol^{-1}$). Therefore, it seems very likely that carbon dioxide produced in the first irreversible step is liberated from the active site at this stage of the catalytic cycle. It is interesting to note that this proposal could provide an explanation for experimental evidence indicating that CO_2 is the first product released from the active site of α-KG-dependent enzymes.[48] Consequently, following the assumption that in the next catalytic steps carbon dioxide is not present in the active site, CO_2 has been excluded from the model. However, since it has been proposed in the literature that succinate and CO_2 could form an anhydride coordinated to iron(IV), the stability of that CO_2-bound form is addressed in the subsection dedicated to the ferryl–oxo species.

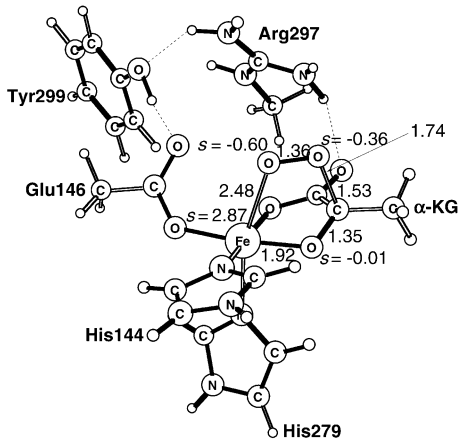

Figure 6. Optimized structure for the triplet superoxo bicyclic complex.

By exploring the triplet potential-energy surface a stable superoxo-bridged structure corresponding to the species **5a** in Scheme 1 has been found. In this complex, shown in Figure 6, three unpaired d electrons on Fe^{III} are antiferromagnetically coupled with one unpaired electron on the dioxygen fragment. The calculated free energy of this complex is, however, quite high ($\Delta G = 24.0\ kcal\,mol^{-1}$, $\Delta H = 17.1\ kcal\,mol^{-1}$, $-T\Delta S = 6.9\ kcal\,mol^{-1}$), which means that this intermediate lies $7.8\ kcal\,mol^{-1}$ above the quintet transition state for the first irreversible step. At this stage it is worthwhile to compare the structures obtained for the quintet and triplet potential-energy surfaces. More specifically, inspection of Figure 4 and Figure 6 reveals that the transition state leading to the Fe^{II}–peracid complex on the quintet PES resembles the stable triplet superoxo bicyclic intermediate. In both cases the dioxygen fragment resembles a superoxide radical both concerning the O–O distance and the spin populations on the oxygen atoms. Therefore, it seems that the electronic configuration of iron governs the stability of these species. In the triplet complex, depicted in Figure 6, one of the 3d orbitals on iron is empty and may form a relatively strong dative bond with an oxygen atom (O3, for numbers see Scheme 1), which becomes negatively charged upon a nucleophilic attack of the superoxo species on the α-keto carbon. In contrast, for the quintet spin state all 3d orbitals on iron are singly occupied, and, therefore, the transition metal (TM) stabilizes the tetrahedral (at C4) intermediate to a lesser extent. Indeed, comparing Figures 4 and 6 we notice that the Fe–O3 distance is notably shorter for the triplet intermediate than for the quintet TS (1.92 Å vs 1.98 Å). This weaker stabilization effect of the TM together with the high exothermicity of the decarboxylation step (see Figure 11, vide infra) results in a spontaneous oxidation of α-KG once the system has achieved the transition-state geometry. Finally, as a comparison, in the catalytic cycle of the radical enzyme pyruvate formate lyase (PFL), a similar tetrahedral intermediate is formed after the attack of a cysteinyl radical on the carbonyl carbon atom of pyruvate.[49,50] However, there is a subtle difference between PFL and the system studied here. In PFL a radical attack of Cys–S$^{\bullet}$ on the carbonyl group leads to a tetrahedral intermediate with a covalent S–C bond and an unpaired electron on the oxygen atom. In contrast, in α-KG-dependent enzymes the superoxide species performs a nucleophilic attack, which means that the O–O fragment retains its superoxide character and the negative charge builds up on the oxygen atom (previously a carbonyl oxygen). Thus, the catalytic role of iron is threefold at this stage of the catalytic cycle of α-KG-dependent enzymes. Firstly, the ferrous ion is necessary to produce the superoxo species. Secondly, the ferric ion seems to stabilize the tetrahedral intermediate with a negative charge accumulated on the oxygen atom originating from the carbonyl group. Finally, the ferric ion is a sink for one of the two electrons released from co-substrate during the C–C bond cleavage, while the second electron reduces the superoxide species to a peroxo moiety.

Starting from the triplet intermediate shown in Figure 6 and following the triplet potential-energy surface a transition state leading to the Fe^{II}–peracid–CO_2 complex was found. In this Fe^{II}–peracid–CO_2 intermediate the ferrous ion is in the triplet spin state. The transition state lies 8.8 kcal mol^{-1} ($\Delta H = 7.8\ kcal\,mol^{-1}$, $-T\Delta S = 1.0\ kcal\,mol^{-1}$) above the superoxo-bridged structure, which means that this triplet transition state lies $16.6\ kcal\,mol^{-1}$ higher than the quintet counterpart. Taken together, the results obtained for the triplet and quintet spin states demonstrate that decarboxylation on the latter PES involves the lower barrier.

For the septet spin state, the oxidative decarboxylation of α-KG would have to proceed directly from the septet Fe–O_2 complex to the high-valent iron–oxo species for two reasons. Firstly, the computational results indicate that the superoxo-bridged septet species (corresponding to **5a** in Scheme 1) does not form. Secondly, a septet spin state for the Fe^{II}–peracid complex will imply that the O–O fragment is in a triplet excited state, and this electronic configuration is most likely at quite high energy. Accordingly, the transition state for the C–C and O–O concerted bond cleavage on the septet PES lies $6.4\ kcal\,mol^{-1}$ higher ($\Delta H = 8.9\ kcal\,mol^{-1}$, $-T\Delta S = -2.5\ kcal\,mol^{-1}$) than the first transition state on the quintet PES. In conclusion, a comparison of the computational results obtained for septet, quintet, and triplet spin

states suggests that on the quintet PES is dioxygen most efficiently activated for oxidative decarboxylation of α-KG.

O–O bond cleavage in the iron(II)–peracid intermediate: The results discussed in the previous subsection support oxidative decarboxylation of α-KG leading from the Fe–O_2 complex directly to the Fe^{II}–peracid intermediate. Thus, in order to generate the high-valent iron(IV) species the O–O bond in the peracid fragment needs to be cleaved. The heterolytic cleavage of the O–O bond is equivalent to a two-electron reduction of the peracid oxygen atoms associated with ferrous ion oxidation to the +4 oxidation state. On the quintet potential-energy surface this process proceeds in two one-electron steps separated by an intermediate characterized by half a bond between the two oxygen atoms. This mechanism has previously been observed for similar systems such as cytochrome c oxidase,[51] a biomimetic iron catalyst[52] and tetrahydrobiopterin-dependent amino acid hydroxylases.[53] The transition state leading to the intermediate in which the O–O bond has not been completely cleaved is shown in Figure 7. The spin on iron is somewhere between the values for the reactant and product of this step (see Figures 5 and 8) and indicates that one electron is being moved from iron to the O–O σ* orbital. The activation free energy for this step amounts to 5.8 kcal mol^{-1} ($\Delta H = 4.9$ kcal mol^{-1}, $-T\Delta S = 0.9$ kcal mol^{-1}) and the process is exothermic by 2.3 kcal mol^{-1} (without thermal effects, since for the small model the intermediate with half a O–O bond is unstable). The structure of the resulting intermediate is depicted in Figure 8. Interestingly, the carbon–oxygen distances in the peracid fragment for the intermediate and the transition state are almost interchanged. Thus, the bond which had previously a double bond character now becomes elongated, while the original single bond shortens. The O–O bond length (2.11 Å) in this intermediate is considerably longer than for the Fe^{II}–peracid complex (1.52 Å), but it still indicates a bonding interaction between the two oxygen atoms.

The second electron transfer proceeds even more readily as the calculated activation energy (without solvent and thermal corrections) amounts to only 0.5 kcal mol^{-1}. The optimized geometry of the second transition state for O–O bond cleavage is shown in Figure 9. Notably, the Fe–O distance increases from 1.78 to 1.83 Å going from the intermediate with half a O–O bond to the second transition state of O–O heterolysis. Moreover, comparing the spins on O1 in Figures 8–10 one can notice that a remarkable negative spin builds up on this atom at the transition state, and then it changes sign and increases at the expense of the spin on iron. In addition, comparison of Figures 8–10 reveals that the second shell arginine facilitates the O–O bond cleavage. At the transition state the arginine is involved in a bifurcated hydrogen bond with both oxygen atoms of the O–O bond, while in the final structure of the high-valent Fe^{IV} species it forms a network of hydrogen bonds with three oxygen atoms. The small activation energy for the second electron transfer causes the process to become activationless when the solvent corrections are added. The second electron transfer is exothermic by 14.2 kcal mol^{-1}, while the whole two-electron process is exergonic by 19.7 kcal mol^{-1} ($\Delta H = -20.3$ kcal mol^{-1}, $-T\Delta S = 0.6$ kcal mol^{-1}). Thus, the O–O bond cleavage process is fast (small activation free energy) and it is irreversible (high exergonicity). The cleavage of the O–O bond leads to the ferryl-oxo quintet species depicted in Figure 10. The short Fe=O bond of 1.65 Å matches very

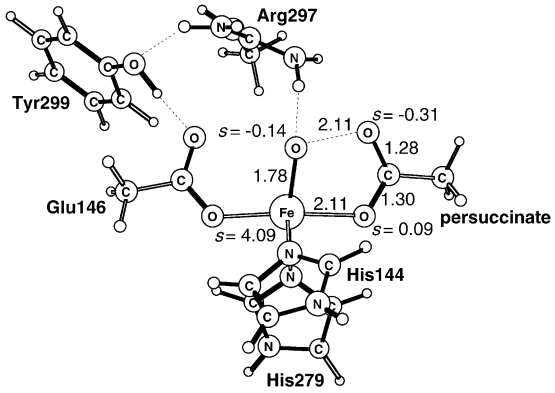

Figure 8. Optimized structure for the quintet intermediate with half a bond between the oxygen atoms.

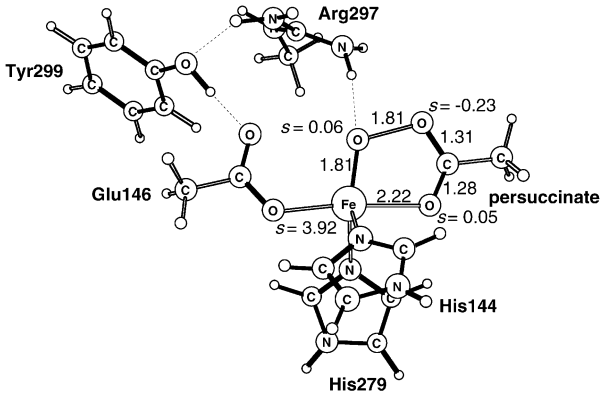

Figure 7. Optimized structure for the first transition state on the quintet potential-energy surface for the O–O bond cleavage.

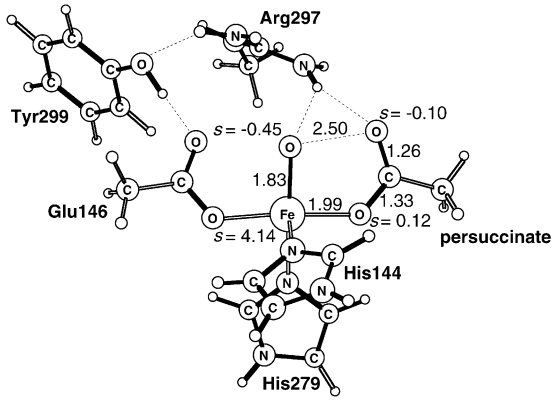

Figure 9. Optimized structure for the second transition state on the quintet potential-energy surface for the O–O bond cleavage.

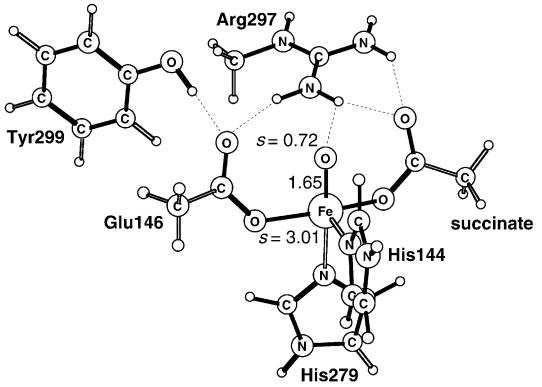

Figure 10. Optimized structure for the quintet ground state of the high-valent iron species Fe^{IV}=O proposed to be involved in oxidative reactions catalyzed by α-KG-dependent enzymes.

Table 2. Relative energies and chosen metric parameters for optimized forms of the high-valent iron-oxo complexes.

Species	ΔG [kcal mol^{-1}]	ΔH [kcal mol^{-1}]	$-T\Delta S$ [kcal mol^{-1}]	Fe–O1 [Å]	Fe–O4 [Å]	Fe–O3 [Å]	C1–O2 [Å]
septet	−57.2	−47.4	−9.8	1.95	–	1.91	–
quintet	−70.6	−62.6	−8.0	1.65	–	1.92	–
triplet	−52.5	−46.6	−5.9	1.63	–	1.95	–
septet–CO_2	−43.8	−44.0	0.2	1.93	2.95	1.94	2.80
quintet–CO_2	−49.8	−51.1	1.3	1.66	2.61	1.93	2.71
septet–anhydride	−35.1	−38.1	3.0	1.95	1.98	2.27	1.51
quintet–anhydride	−44.2	−48.1	3.9	1.65	2.00	2.22	1.55

well the one observed in the crystal structure of the non-heme iron(IV) complex (1.646(3) Å).[38] The electronic structure and relative stability of various possible forms of the high-valent iron–oxo species is discussed in the next subsection.

High-valent iron–oxo species: As described above, the O–O bond heterolysis leads from the peracid intermediate to the high-valent Fe^{IV} species. As for the loosely bound dioxygen complexes, there are also in this case several possible spin states. Additionally, the possibility of CO_2 binding to iron, either in the "native" form or as an anhydride with succinate, complicates the picture further. In an attempt to gain some insight into the relative stability of various forms of high-valent Fe^{IV} intermediates the structures of the septet, quintet, and triplet complexes without CO_2, with CO_2 bound to iron, and with the CO_2–succinate anhydride were optimized. Only the structure with the "native" CO_2 bound to iron in a triplet spin state turned out to be impossible to optimize. In this case, the optimization leads directly to the C1–O2 bond formation (for atom numbering see Scheme 1), which means that for the triplet spin state CO_2 binds to iron only in the form of an anhydride with succinate. It seems likely that this behavior, peculiar to the triplet spin state, reflects the electronic structure of the iron complex. For that spin multiplicity Fe^{IV} has one empty d orbital, and this orbital participates in a dative bond from the anionic anhydride stabilizing the structure with a covalent bond between CO_2 and succinate. The energies and most relevant geometrical parameters for the optimized forms of the ferryl–oxo species are gathered in Table 2. Analysis of the data in Table 2 reveals that the quintet five-coordinate complex is the ground state for the high-valent iron–oxo species in the active site of clavaminic acid synthase. Binding of carbon dioxide to the Fe^{IV} site is endergonic, and anhydride formation does not stabilize it. Thus, the conclusion that CO_2 leaves the active site soon after it is formed (vide supra) gains further support here. Neither the Fe^{II} nor the Fe^{IV} species formed along the catalytic reaction path bind carbon dioxide. The crystal structures obtained for ANS–α-KG–substrate complex before and after dioxygen exposure are consistent with this conclusion.[15] In the latter case, the product and the succinate are bound to iron, while carbon dioxide has been substituted by a water molecule. In contrast, the crystal structure of the DAOCS ΔR07A mutant (1E5H)[17] reveals a CO_2 bound to the ferrous site, in which a succinate is also found in the first coordination sphere of iron. However, this complex has not been obtained as a product of the catalytic reaction, and, therefore, it may have limited relevance in the discussion of the species formed along the catalytic reaction path.

Finally, a note about the electronic structure of the high-valent Fe^{IV} species. Taking into account only the most relevant atomic orbitals of the Fe=O fragment (2p on oxygen, 3d on iron), eight molecular orbitals can be constructed for this fragment: σ, σ*, two π, two π*, and two non-bonding δ orbitals localized on iron. These orbitals accommodate ten electrons leading to the following electronic configurations for the three multiplicities: triplet $(\sigma)^2(\pi_a)^2(\pi_b)^2(\delta_a)^2(\pi^*_a)^1(\pi^*_b)^1$, quintet $(\sigma)^2(\pi_a)^2(\pi_b)^2(\delta_a)^1(\delta_b)^1(\pi^*_a)^1(\pi^*_b)^1$, and septet $(\sigma)^2(\pi_a)^2(\pi_b)^1(\delta_a)^1(\delta_b)^1(\pi^*_a)^1(\pi^*_b)^1(\sigma^*)^1$. Notably, the triplet and quintet spin states differ only in the pairing of the electrons occupying the non-bonding d orbitals on iron. Therefore, the Fe–O bond length in these two species is very similar (1.63 Å for the triplet, 1.65 Å for the quintet), as is the spin on the oxygen atom (0.86 for the triplet, 0.72 for the quintet). The formal Fe–O bond order amounts to two for the triplet and quintet species. As regards the septet spin state, the $\pi \rightarrow \sigma^*$ triplet excitation, which formally leads from the quintet to the septet state, leads to a Fe–O bond elongation (1.95 Å). This significant bond length increase can be rationalized by a formal Fe–O bond order equal to one, as calculated from the above electronic configuration. Since for the septet state twice as many (alpha) unpaired electrons occupy the Fe–O bonding and antibonding molecular orbitals as in the quintet and triplet states, the spin on oxygen almost doubles (1.30 for the septet vs 0.72 for the quintet).

Conclusions

The results of hybrid density functional calculations that are reported here show that dioxygen activation in α-KG-dependent enzymes proceeds most efficiently on the quintet potential-energy surface. The energetics of the proposed reaction mechanism are summarized in Figure 11. Briefly, consistent with the experimental data, the decarboxylation reaction is found to be irreversible and CO_2 leaves the active site once it is produced, that is, it is the first product released. Moreover, this step, in which the Fe^{II}–peracid intermediate is formed and α-KG is oxidatively decarboxylated, is found to be rate-limiting. This finding together with the small activation barriers for the following steps explain why the peracid intermediate is not observed experimentally. The O–O bond cleavage in the Fe^{II}–peracid intermediate takes place in two one-electron steps, and produces the high-valent iron–oxo species. The low calculated activation free energy and significant exergonicity of this step imply that the O–O bond breaking is very quickly completed under ambient temperatures. Finally, the ground state for the ferryl–oxo species has been found to be a pentacoordinate quintet complex. On the septet potential-energy surface the dioxygen activation process is less efficient (a barrier higher by 6.4 kcal mol^{-1}) and proceeds through a transition state for a concerted O–O and C–C bond cleavage. The mechanism of dioxygen activation that is suggested here for α-KG-dependent enzymes has striking analogies to the catalytic process of dioxygen cleavage in tetrahydrobiopterin-dependent amino acid hydroxylases.[53] In both cases the reaction advances on the quintet potential-energy surface and the process starts with dioxygen binding to the ferrous five-coordinate active site. Furthermore, in both cases dioxygen bound to the iron site is reduced to the peroxo species in a rate-limiting step, and the O–O bond cleavage passes through two one-electron steps both in α-KG- and tetrahydrobiopterin-dependent enzymes. Thus, despite the different chemical character of the cofactors, a common theme for dioxygen activation has been found for these two classes of non-heme iron dioxygenases.

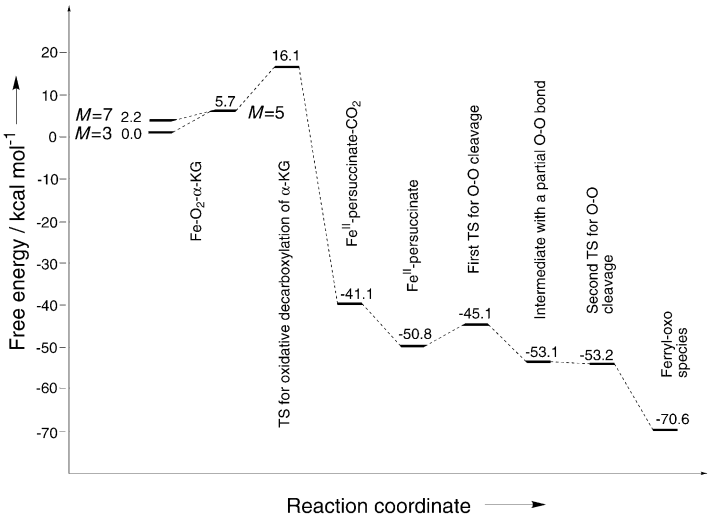

Figure 11. Free-energy profile for the suggested mechanism of dioxygen activation in α-KG-dependent enzymes.

Acknowledgement

The authors want to thank M. Mehn and co-authors for a preprint of reference [33].

[1] M. Ivan, K. Kondo, H. Yang, W. Kim, J. Valiando, M. Ohh, A. Salic, J. M. Asara, W. S. Lane, W. G. Kaelin, Jr., *Science* **2001**, *292*, 464–468.
[2] P. Jaakkola, D. R. Mole, Y. M. Tian, M. I. Wilson, J. Gielbert, S. J. Gaskell, A. von Kriegsheim, H. F. Hebestreit, M. Mukherji, C. J. Schofield, P. H. Maxwell, C. W. Pugh, P. J. Ratcliffe, *Science* **2001**, *292*, 468–472.
[3] S. C. Trewick, T. F. Henshaw, R. P. Hausinger, T. Lindahl, B. Sedgwick, *Nature* **2002**, *419*, 174–178.
[4] P. Ø. Falnes, R. F. Johansen, E. Seeberg, *Nature* **2002**, *419*, 178–182.
[5] P. A. Aas, M. Otterlei, P. ø. Falnes, C. B. Vågbø, F. Skorpen, M. Akbari, O. Sundheim, M. Bjørås, G. Slupphaug, E. Seeberg, H. E. Krokan, *Nature* **2003**, *421*, 859–863.
[6] A. G. Prescott, M. D. Lloyd, *Nat. Prod. Rep.* **2000**, *17*, 367–383.
[7] M. J. Ryle, R. P. Hausinger, *Curr. Opin. Chem. Biol.* **2002**, *6*, 193–201.
[8] S. J. Lange, L. Que, Jr., *Curr. Opin. Chem. Biol.* **1998**, *2*, 159–172.
[9] L. Que, Jr., R. Y. N. Ho, *Chem. Rev.* **1996**, *96*, 2607–2624.
[10] A. L. Feig, S. J. Lippard, *Chem. Rev.* **1994**, *94*, 759–805.
[11] C. J. Scholfield, Z. Zhang, *Curr. Opin. Struct. Biol.* **1999**, *9*, 722–731.
[12] E. S. Solomon, T. C. Brunold, M. I. Davis, J. N. Kemsley, S. K. Lee, N. Lehnert, F. Neese, A. J. Skulan, Y. S. Yang, J. Zhou, *Chem. Rev.* **2000**, *100*, 235–349.
[13] Z. Zhang, J. Ren, D. K. Stammers, J. E. Baldwin, K. Harlos, C. J. Schofield, *Nat. Struct. Biol.* **2000**, *7*, 127–133.
[14] I. J. Clifton, L. C. Hsueh, J. E. Baldwin, K. Harlos, C. J. Scholfield, *Eur. J. Biochem.* **2001**, *268*, 6625–6636.
[15] R. C. Wilmought, J. J. Turnbull, R. W. D. Welford, I. J. Clifton, A. G. Prescott, C. J. Schofield, *Structure* **2002**, *10*, 93–103.
[16] K. Vålegard, A. C. Terwisscha van Scheltinga, M. D. Lloyd, T. Hara, S. Ramaswamy, A. Perrakis, A. Thompson, H. J. Lee, J. E. Baldwin, C. J. Schofield, J. Hajdu, I. Andersson, *Nature* **1998**, *394*, 805–809.
[17] H. J. Lee, K. Lloyd, M. D. Harlos, I. J. Clifton, J. E. Baldwin, C. J. Schofiel, *J. Mol. Biol.* **2001**, *308*, 937–948.
[18] L. Serre, A. Sailland, D. Sy, P. Boudec, A. Rolland, E. Pebay-Peyroula, C. Cohen-Addad, *Structure* **1999**, *7*, 977–988.
[19] L. Que, Jr., *Nat. Struct. Biol.* **2000**, *7*, 182–184.
[20] E. G. Pavel, J. Zhou, R. W. Busby, M. Gunsior, C. A. Townsend, E. I. Solomon, *J. Am. Chem. Soc.* **1998**, *120*, 743–753.
[21] J. Zhou, W. L. Kelly, B. O. Bachmann, M. Gunsior, C. A. Townsend, E. I. Solomon, *J. Am. Chem. Soc.* **2001**, *123*, 7388–7398.
[22] E. I. Solomon, A. Decker, N. Lehnert, *Proc. Natl. Acad. Sci. USA* **2003**, *100*, 3589–3594.
[23] L. D. Thornburg, M. T. Lai, J. S. Wishnok, J. Stubbe, *Biochemistry* **1993**, *32*, 14013–14033.
[24] J. E. Penner-Hahn, K. S. Eble, T, J. McMurry, M. Renner, A. L. Balch, J. T. Groves, J. H. Dawson, K. O. Hodgson, *J. Am. Chem. Soc.* **1986**, *108*, 7819–7825.
[25] I. Schlichting, J. Berendzen, K. Chu, A. M. Stock, S. A. Maves, D. E. Benson, R. M. Sweet, D. Ringe, G. A. Petsko, S. G. Sligar, *Science* **2000**, *287*, 1615–1622.
[26] J. C. Price, E. W. Barr, B. Tirupati, J. M. Bollinger, Jr., C. Krebs, *Biochemistry* **2003**, *42*, 7497–7508.
[27] D. F. Counts, G. J. Cardinale, S. Udenfriend, *Proc. Natl. Acad. Sci. USA* **1987**, *84*, 2145–2149.
[28] G. J. Cardinale, S. Udenfriend, *Adv. Enzymol. Relat. Areas Mol. Biol.* **1974**, *41*, 245–300.

[29] M. J. Ryle, A. Liu, R. B. Muthukumaran, R. Y. N. Ho, K. D. Koehntop, J. McCracken, L. Que, Jr., R. P. Hausinger, *Biochemistry* **2003**, *42*, 1854 – 1862.
[30] Z. Zhang, J. Ren, K. Harlos, C. H. McKinnon, I. J. Clifton, C. J. Schofield, *FEBS Lett.* **2002**, *517*, 7 – 12.
[31] Y. M. Chio, L. Que, Jr., *J. Am. Chem. Soc.* **1995**, *117*, 3999 – 4013.
[32] E. H. Ha, R. Y. N. Ho, J. F. Kisiel, J. S. Valentine, *Inorg. Chem.* **1995**, *34*, 2265 – 2266.
[33] M. P. Mehn, K. Fujisawa, E. L. Hegg, L. Que, Jr., *J. Am. Chem. Soc.* **2003**, *125*, 7828 – 7842.
[34] J. San Filippo, Jr., L. J. Romano, C. I. Chern, J. S. Valentine, *J. Org. Chem.* **1976**, *41*, 586 – 588.
[35] J. San Filippo, Jr., C. I. Chern, J. S. Valentine, *J. Org. Chem.* **1976**, *41*, 1077 – 1078.
[36] E. L. Hegg, R. Y. N. Ho, L. Que, Jr., *J. Am. Chem. Soc.* **1999**, *121*, 1972 – 1973.
[37] S. J. Lange, H. Miyake, L. Que, Jr., *J. Am. Chem. Soc.* **1999**, *121*, 6330 – 6331.
[38] J. U. Rohde, J. H. In, M. H. Lim, W. W. Brennessel, M. R. Bukowski, A. Stubna, E. Münck, W. Nam, L. Que, Jr., *Science* **2003**, *299*, 1037 – 1039.
[39] P. E. M. Siegbahn, *Q. Rev. Biophys.* **2003**, *36*, 91 – 145.
[40] A. D. J. Becke, *J. Chem. Phys.* **1993**, *98*, 5648 – 5652.
[41] C. Lee, W. Yang, R. G. Parr, *Phys. Rev.* **1988**, *37*, 785 – 789.
[42] *Gaussian 98*, Revision A.1, M. J. Frisch, G. W. Trucks, H. B. Schlegel, G. E. Scuseria, M. A. Robb, J. R. Cheeseman, V. G. Zakrzewski, J. A. Montgomery, Jr., R. E. Stratmann, J. C. Burant, S. Dapprich, J. M. Millam, A. D. Daniels, K. N. Kudin, M. C. Strain, O. Farkas, J. Tomasi, V. Barone, M. Cossi, R. Cammi, B. Mennucci, C. Pomelli, C. Adamo, S. Clifford, J. Ochterski, G. A. Petersson, P. Y. Ayala, Q. Cui, K. Morokuma, D. K. Malick, A. D. Rabuck, K. Raghavachari, J. B. Foresman, J. Cioslowski, J. V. Ortiz, B. B. Stefanov, G. Liu, A. Liashenko, P. Piskorz, I. Komaromi, R. Gomperts, R. L. Martin, D. J. Fox, T. Keith, M. A. Al-Laham, C. Y. Peng, A. Nanayakkara, C. Gonzalez, M. Challacombe, P. M. W. Gill, B. G. Johnson, W. Chen, M. W. Wong, J. L. Andres, M. Head-Gordon, E. S. Replogle, J. A. Pople, Gaussian, Inc., Pittsburgh PA, **1998**.
[43] JAGUAR 4.0, Schrödinger, Inc., Portland, Oregon, **2000**.
[44] D. J. Tannor, B. Marten, R. Murphy, R. A. Friesner, D. Sitkoff, A. Nicholls, M. Ringnalda, W. A. Goddard III, B. Honig, *J. Am. Chem. Soc.* **1994**, *116*, 11 875 – 11 882.
[45] B. Marten, K. Kim, C. Cortis, R. A. Friesner, R. Murphy, M. Ringnalda, D. Sitkoff, B. Honig, *J. Phys. Chem.* **1996**, *100*, 11 775 – 11 788.
[46] M. Wirstam, S. J. Lippard, R. A. Friesner, *J. Am. Chem. Soc.* **2003**, *125*, 3980 – 3987.
[47] M. J. Ryle, R. Padmakumar, R. P. Hausinger, *Biochemistry* **1999**, *38*, 15 278 – 15 286.
[48] E. Holme, *Biochemistry* **1975**, *14*, 4999 – 5003.
[49] F. Himo, L. A. Eriksson, *J. Am. Chem. Soc.* **1998**, *120*, 11 449 – 11 455.
[50] F. Himo, P. E. M. Siegbahn, *Chem. Rev.* **2003**, *103*, 2421 – 2456.
[51] M. R. A. Blomberg, P. E. M. Siegbahn, M. Wikström, *Inorg. Chem.* **2003**, *42*, 5231 – 5243.
[52] A. Bassan, M. R. A. Blomberg, P. E. M. Siegbahn, L. Que, Jr., *J. Am. Chem. Soc.* **2002**, *124*, 11 056 – 11 063.
[53] A. Bassan, M. R. A. Blomberg, P. E. M. Siegbahn, *Chem. Eur. J.* **2003**, *9*, 106 – 115.

Received: July 4, 2003
Revised: September 4, 2003 [F5306]

